# Cancellation of Biodynamic Feedthrough in Vehicle Control Tasks

Szabolcs Sövényi and R. Brent Gillespie

***Abstract*— Biodynamic feedthrough refers to the transmission of vehicle motion from the seat through the driver's body to the steering or speed control interface where it produces unintended vehicle control commands. This pathway through the body closes a feedback loop that degrades driving performance and can even produce sustained oscillations in the human-vehicle system. In certain instances these oscillations can jeopardize vehicle safety. In this paper we propose and test a model-based cancellation controller to mitigate the effects of biodynamic feedthrough. The biodynamic model is constructed in a preliminary system identification experiment in which vehicle acceleration and control interface interaction force are measured. The system identification experiment is carefully designed to capture the biodynamic transmittance rather than the driving point impedance at the control interface. In operation, the controller processes vehicle acceleration measurements through a transfer function model of the human biodynamics and a motor imposes the result as a torque that acts directly on the manual control interface. We investigated the efficacy of model-based cancellation by quantifying the manual performance of 12 human subjects using a joystick to control displacements of a single-axis motion platform upon which they were seated. Biodynamic models were individually fit and tested as cancellation controllers for each subject. Comparing performance with and without cancellation in place, the cancellation controller reduced oscillation spectral energy in the 1-7Hz band by 75 % and reduced the root mean square tracking error by 44 %. The cancellation controller also had a positive effect on the disturbance response of the driver-vehicle system.**

***Index Terms*— biodynamic feedthrough, vibration feedthrough, McRuer's crossover model, pursuit tracking, force reflecting interface, roll-ratchet.**

## I. Introduction

When piloting an aircraft, driving a ground vehicle, or even when steering a boat, the operator's body is subjected to motions of the vehicle, usually transferred through a seat. On the one hand, vehicle motion can be helpful since it serves as a cue to inform the operator about the behavior of the vehicle. On the other hand however, vehicle motion can be a hindrance to piloting performance. Although increased cognitive load or perceptual overload may be a factor, another phenomenon, called biodynamic feedthrough can have a significant impact without involving volitional control at all [1]. Vehicle motions are transmitted through the body of the operator and vehicle accelerations induce inertia forces that act on the manual control interface, quite outside the intentions of the operator.

Manuscript submitted August 2005, IEEE Transactions on Control Systems Technology;

S. Sövényi and R.B. Gillespie are both with the Department of Mechanical Engineering, University of Michigan

When the operator grasps a manual interface to close a control loop and express his intentions, a second, purely mechanical feedback loop is closed through the operator's trunk, arm, and hand. The vehicle accelerations can then act through the operator's body to produce joystick motions that in turn influence vehicle motion. Oscillations may appear in the human-machine system—oscillations that may grow unchecked given sufficient loop gain and accumulated phase difference between vehicle motion and biodynamic response. Often the amplitude and frequency of the oscillations preclude their suppression by volitional control of the operator.

Biodynamic feedthrough is recognized as a threat to safe operation of hydraulically actuated booms or diggers used in forestry or construction equipment [2] [3], as the cause of oscillatory roll motion called roll-ratchet in modern fighter jets [4], and oscillatory bucking motion in powered wheelchairs [5]. Biodynamic feedthrough can also play a role in inciting or exacerbating oscillations in the feedback loop in which the pilot acts as controller. These oscillations, resulting from compromised stability in the pilot-controlled loop are called Pilot Induced Oscillations (PIO). Time delays between the action and perceived response of the controlled element are at the root of PIO, and occasionally the gain or phase margins can be exceeded when the PIO loop is coupled with or disturbed by feedthrough dynamics [6].

Biodynamic feedthrough also plays a role in the scenario in which the operator uses the manual interface to control not the vehicle, but another machine. In this case the operator's body does not close a mechanical feedback loop. Rather, biodynamic feedthrough acts as a disturbance signal that impedes manual control performance involving the machine. We have modeled and experimentally investigated biodynamic feedthrough in the machine-control (rather than vehicle-control) case in a companion paper [7].

### A. Biodynamic System Models

A number of biodynamic system models have appeared in the literature, and these can be arranged roughly into two groups: multibody models and black box models. Some of the multibody models, including [2], [8], [9] and [10] are in fact very simple, using only a mass-spring-damper representation of the the operator's body. In [4], a simple inertial component was augmented with a time delay to model phase lags associated with high frequency dynamics. A more elaborate model is constructed for a semisupine pilot in [11].

In this paper we empirically fit a black box model to the biodynamic system, using data from a carefully crafted system

identification experiment that targets aspects of the biodynamic behavior most relevant to biodynamic feedthrough. We use an autoregressive moving average (ARMA) model with four poles and four zeros to describe the transfer function from vehicle acceleration to unintended joystick force. This model is fit individually to data collected from each of our human subjects in a system identification experiment whose protocol is based in turn on a block diagram model of human-vehicle system. Our block diagram model carefully distinguishes between two transfer functions within the biomechanical system: the transmittance between vehicle seat and manual interface and the driving point impedance at the manual interface. This feature improves upon the models that have appeared to date, including [10] and [8].

### *B. Solution Approaches*

Certain features of the vehicle interface can be used to mitigate biodynamic feedthrough, including restraint systems to immobilize the trunk, elbow rests [1], or ensuring that the axes of motion within the manual interface are not aligned with the predominant directions of vehicle motion. A steering wheel, for example, is not generally sensitive to lateral motion, especially when gripped in the 3 and 9 o'clock positions. Nevertheless, high-performance vehicles may be sensitive to biodynamic feedthrough despite the incorporation of these mitigating design features. For example, elbow rests were not sufficient to suppress the effects in highly maneuverable jet aircraft [4].

When restraints, armrests, and re-alignment of the interface displacement axes are either not available or not sufficient to remove biodynamic feedthrough effects, two additional approaches remain. The first of these is to suppress the effects of biodynamic feedthrough by modifying the mechanical impedance of the interface or by decreasing the gain on the signal from manual interface to vehicle command. The addition of damping to the interface and a lowered gain proved sufficient in a simulation study in [2]. The success of this approach, however, relies on a bandwidth separation between the dynamics of biodynamic feedthrough and the manual control loop. If a clear bandwidth separation does not exist, then modifying the mechanical impedance of the interface or lowering the gain to suppress the effects of biodynamic feedthrough will also tend to suppress the control signal produced by the human.

An alternative approach that targets the biodynamic effects directly is based on cancellation. A signal generated electronically using a transfer function operating on a measure of vehicle acceleration can be injected into the human-vehicle system with an appropriate sign to cancel the effects generated physically. Cancellation has been used in [12], [10] and [8]. Merhav et.al. proposed and tested a cancellation approach in simulation [12] and verified the approach in a multi-axis human subject experiment with 5 subjects in [13]. Their cancellation signal was produced by filtering measured vehicle acceleration through an adaptive high-pass filter. The filter, however, was not based on an identified model of the operator biodynamic feedthrough function and as the authors note, success of the approach hinged on spectral separation between the biodynamic and intentionally produced components of the joystick signal.

In an approach proposed in [8] and significantly extended in [14], a measured vehicle acceleration is fed through a transfer function based explicitly on a model estimate of the biodynamic feedthrough function to produce the cancellation signal. In each of these studies, the model estimate was constructed from data collected in a separate system identification experiment conducted prior to verification of the cancellation controller. Another feature common to the work of [8] and [14] that distinguishes it from earlier work was the injection of the cancelling signal through a motor coupled directly to the joystick. In [10], the feel of the joystick was addressed alongside the problem of biodynamic feedthrough cancellation in a model-matching framework and the design of a controller by mu-synthesis.

### *C. The Proposed Model and Solution*

As in [8] and [14], we use a model-based cancellation approach, basing the cancellation controller on a model constructed in a separate, prior human subject experiment. In contrast to the previous work, however, we use a biodynamic model (also elaborated in [7]) that distinguishes between the transmittance and driving point impedance and a system identification experiment that targets only the transmittance. The experiment used to construct the model makes use of the same vehicle motion simulator and joystick used in verification, but with the joystick immobilized with a peg and outfitted with a force sensor. The model is obtained as a least-squares fit to the vehicle acceleration and manual interface interaction force data recorded for each human subject. Due to non-trivial differences between models across our subjects, we based the cancellation model for each subject on their own biodynamic function estimate. We inject the cancellation signal into the biodynamic system using a DC motor on the joystick.

We demonstrate the effectiveness of the cancellation controller in a human subject experiment with 12 subjects. Within these experiments, we record human performance in a pursuit tracking task to quantify the impact of the cancellation controller. During the tests, the human subject tracks a random-appearing reference signal by commanding platform motion with the joystick. In two conditions, with and without the cancellation compensator, we characterize performance using four metrics. Our protocol also includes a periodic exogenous disturbance signal that allows us to characterize the influence of the cancellation controller on the disturbance response of the system.

In this paper we will focus our attention on vehicles controlled by joysticks, in particular *displacement sticks* (also called *motion sticks*) that produce command signals according to their displacement. Our methods can be extended to the sister class of joysticks, called *force sticks* (also: *stiff sticks*), that produce command signals as a function of force applied to the grip [15].

This paper is organized as follows. In Section II we develop a model for the human-machine system that leads to a system

identification test protocol and our feedthrough cancellation concept. The apparatus and experimental methods pertaining to two experiments are described in Section III. The first experiment is a system identification of the biodynamic model and the second experiment is aimed at quantifying the impact on tracking performance of a cancellation controller based on the identified biodynamic model. Results for both experiments are presented in Section IV. Section VI elaborates on the conclusions and outlines future work.

## II. Modeling the Human-Vehicle System

In this section we develop a mathematical model of the human-vehicle system for use in analyzing the deleterious effects of biodynamic feedthrough on manual tracking performance. Naturally, the most interesting part of the model is the portion that describes the human operator, in particular because the operator plays multiple roles in the system. First, the operator acts as a controller, sending command signals to the vehicle in response to information perceived from the environment. This process is volitional, involving some amount of cognitive processing and voluntary muscle action to steer the vehicle to follow a road or other moving target seen in the environment. This role may be called *volitional tracking* or simply *tracking*.

In his second role, the operator acts, quite inadvertently, as a pathway for disturbance to enter the tracking control loop. His body, being subjected to motion of the vehicle, couples mechanical energy from the vehicle into the manual control interface. This process is called *biodynamic feedthrough* or *biodynamic coupling*, and it does not involve any perception or volitional action on the part of the operator.

To begin the development of our model, we make a few simplifying assumptions about vehicle driving that preserve the relationship between the vehicle and the operator in his two roles. First, as in studies [16], [10], [17], [18] and [1], we reduce the multi-axis ride motion experienced by the driver to motion along a single axis. Likewise, we assume that the manual control interface is configured such that the handle grasped by the operator moves parallel to the ride motion. A single-axis joystick with sufficiently long handle or small displacement angles meets this assumption when the joystick axis of rotation is perpendicular to the motion axis. Support for a model restricted to a single axis is based on the observation that biodynamic feedthrough, when it occurs in real vehicles, does not involve significant coupling between motion axes. Second, we simplify the visual scene of a curving roadway or moving target down to motion of a box on a computer monitor, given without preview. Similarly, the view of the vehicle itself is reduced to a moving cursor on the screen. Tracking tasks without preview are commonly used to model vehicle control problems, e.g. in [19]. Finally, we assume that the human tracking controller can be adequately fit by a quasi-linear model and that the vehicle and biodynamic systems are linear, so that superposition holds. Specifically, the behaviors of the system in response to the operator in each of his two roles (tracking control and biodynamic coupling) are assumed to superpose.

Figure 1 presents a block diagram of the human-vehicle system model. A significant feature of the block diagram is the presence of one feedback loop for each of the two roles played by the driver. The lower feedback path models visual feedback of the vehicle position $x_r$ and forms the loop labelled *tracking loop*. The upper feedback path models biodynamic feedthrough; it feeds the response of the transfer function $H$ to vehicle acceleration $\ddot{x}_v$ and forms the loop labelled *biodynamic loop*.

The transfer function $T$ describes the actions of the driver intended to produce tracking of the reference $x_r$ by the vehicle position $x_v$. Specifically, the transfer function $T$ acts on the difference $x_e$ produced by comparing $x_v$ to the reference $x_r$ and generates a tracking force $f_t$ that is applied on the joystick $J$. Note that we have assumed the tracking controller $T$ uses only visual and not haptic or motion (vestibular) signals. Transfer function $T$ models volitional tracking and will be described in detail in section II-A below. In addition to $f_t$, however, two additional force components act on $J$. The first of these is the biodynamic force $f_b$, the response of $H$. The second component is $f_{jb}$, which is the response of the driver's hand/arm to motions of the joystick. The transfer function $Z$ is the driving point impedance of the human hand/arm and forms an inner feedback loop around the joystick $J$. We show $Z$ explicitly in the model to feature its distinction from $H$, the transmittance. Both $Z$ and $H$ are parts of the human biomechanics. See [7] for an explicit presentation of the modeling steps that produce $H$ and $Z$ from a two-port model of the human operator biomechanics. The sum of $f_t$, $f_b$, and $f_{jb}$ is the total force $f$ that acts on the joystick $J$.

The transfer functions $T$, $H$ and $Z$ model the various functions of the driver, where $T$ includes perception and volitional action, and $H$ and $Z$ include strictly biomechanical responses. The remaining portions of the block diagram model the manual control interface and the vehicle. The joystick $J$, modeled as an admittance, responds with an angular velocity $\dot{x}_j$ to the total force $f$. The joystick angle $x_j$ is multiplied by the scaling factor $C_p$ to obtain a platform position command $x_c$. The vehicle $V$ responds to $x_c$, but also to the additive signal $d$, which models disturbance effects such as wind gusts.

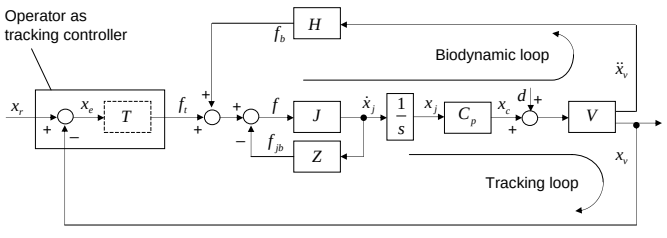


Fig. 1. A block diagram of the human-machine system shows a tracking loop that models a tracking controller $T$ acting through the joystick $J$ to cause the position $x_v$ of the vehicle $V$ to track a reference signal $x_r$. The biodynamic loop containing $H$ models the disrupting effects of biodynamic feedthrough. The transfer function $Z$ models the driving point impedance of the human arm/hand grasping the joystick $J$.

### A. Volitional tracking

The scenario in which a human operator visually monitors a target that moves in an unpredictable fashion and attempts to follow with a cursor or crosshairs that moves under manual control is known as pursuit tracking. Pursuit tracking has been studied extensively since World War II, especially in association with aircraft pilot behavior [20]. One of the best known models of tracking behavior is known as McRuer's crossover model [21], [22]. Part of the utility of the crossover model derives from its indirect approach to describing the human tracking controller $T$. Instead of an explicit description of $T$, it describes the open-loop transfer function of the tracking loop. In Figure 1, the open loop transfer function is the forward path from $x_e$ to vehicle response $x_v$.

McRuer's crossover model is expressed in the frequency domain, giving the gain and phase of the open loop transfer function as a function of frequency in the signals $x_v$ and $x_e$. In its simplest form, The crossover model states that the open-loop transfer function can be described as the product of a constant $\omega_c$, an integrator, and a pure time delay. Referring to Figure 1, if the feedback combination of $J$ and $Z$ is lumped together with $1/s$ and gain $C_p$ into the transfer function $J_Z$, the crossover model reads:

$$T(j\omega)J_Z(j\omega)V(j\omega) = \frac{\omega_c e^{-j\omega T_d}}{j\omega} \tag{1}$$

where $\omega_c$, called the *crossover frequency*, is the frequency at which the magnitude of the open-loop transfer function is unity or $0\,\text{dB}$. The integrator $1/j\omega$ establishes good tracking below the crossover frequency in the closed loop system. Above the crossover frequency, tracking performance in the closed loop system degrades with a $-20$ dB/decade roll-off. Like an experienced control engineer applying Bode design principles might choose for an automatic controller design, the $1/j\omega$ determines a suitable tradeoff between tracking performance with closed loop bandwidth $w_c$ and stability margin. Stability margin is an important consideration, since a good portion is consumed by the time delay $T_d$, which accounts for cognitive and sensorimotor processes. The expression on the right hand side of Equation (1) describes the open loop transfer function in a 1 to 1.5 decade range centered roughly at the crossover frequency $w_c$.

The motivation for modeling the open loop system rather than focusing on the transfer function $T$ is that the crossover model fits many different plant types. The crossover model says that the human operator adapts to the plant, and to whatever extent dictated by the plant dynamics, inverts it so that the open-loop transfer function becomes $1/j\omega$. Based on extensive human subject experiments, values for $w_c$ and $T_d$ have been determined for various plant types (whether $V$ is a gain, an integrator, double-integrator, and so-on) and tabulated in the literature [20].

In this paper we will use the crossover model to characterize the tracking performance of the human operator under various experimental conditions involving ride motion disturbance and/or compensation. Specifically, we will determine a crossover frequency for each subject and each condition by fitting a crossover model to the performance data.

### B. Model-based feedthrough cancellation

To mitigate the effects of biodynamic feedthrough, we propose to apply a cancellation force $\hat{f}_b$ to the joystick in a direction that opposes $f_b$ through the action of a motor coupled directly to the joystick. The command signal for the motor will be produced by an estimate $\hat{H}$ for the biodynamic transfer function $H$ and a measure (through an accelerometer) of the vehicle acceleration $\ddot{x}_v$. Figure 2 presents a simplified version of the block diagram appearing in Figure 1 along with an additional feedback path representing the compensator based on $\hat{H}$. The simplifications embodied in Figure 1 include the lumping together of the feedback combination of $J$ and $Z$ with the integrator $1/s$ and gain $C_p$.

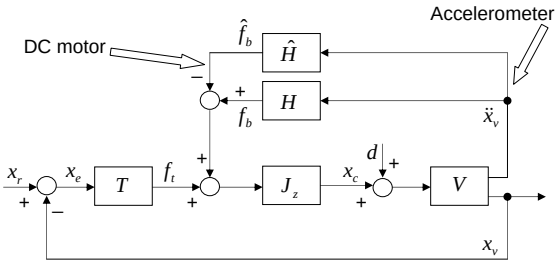


Fig. 2. In our proposed compensation approach, the effects of biodynamic feedthrough are cancelled with a force $\hat{f}_b$ computed based on an estimate $\hat{H}$ of the biodynamic feedthrough transfer function and a measure of vehicle acceleration $\ddot{x}_v$. The force $\hat{f}_b$ is to be applied to the joystick through the action of a DC motor.

## III. Methods

*1) Apparatus:* While the hardware and software for transfer functions $T$, $H$, and $Z$ of Figure 1 are supplied, in effect, by our human subjects, hardware and software for the remaining components is supplied by our apparatus. There are three chief components to the apparatus, a manual control interface (the joystick $J$), a motion platform (the vehicle $V$), and a monitor for visual display. These three components are depicted together with a human subject in Figure 3.

**Hardware**

The platform produced ride motion for a human subject seated and buckled with a five-point harness in a racing car seat. The seat was mounted such that motion was in the lateral direction, or aligned horizontally in the frontal plane of the subject. The platform moved within a $\pm 0.15\,\text{m}$ workspace, driven by a 2.24 kW brushless DC servo motor (Koll Morgan Goldline B 404-B-A3) through a ball screw. A high resolution resolver read angular position for a computer controller.

A single-axis joystick mounted to the platform within reach of the human subject's right hand serves as a manual control interface for the subject. The joystick is mounted such that the small-motion displacements of the joystick handle and platform displacements are aligned. The joystick is a modified version of the IE2000 haptic interface from Immersion Corporation. The two-axis IE2000 has been reconfigured as a single axis joystick by removing the spherical kinematic mechanism

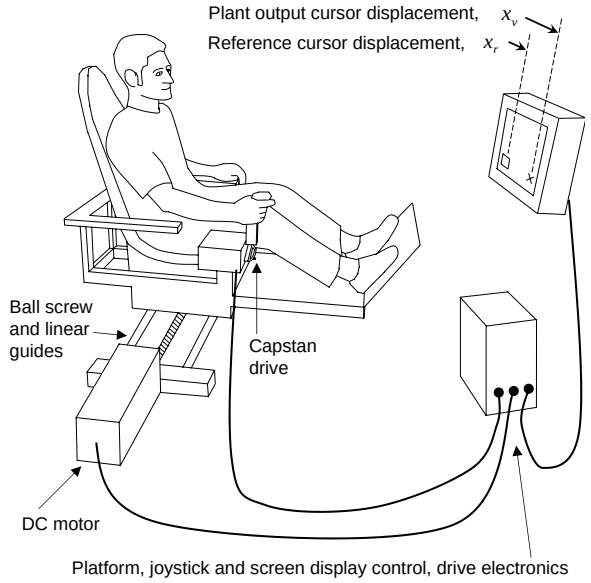


Fig. 3. A human operator seated on a single-axis motion platform uses a joystick to move the platform so as to make a cursor representing platform position on the screen track a target that moves in an unpredictable fashion.

and the motor has been replaced with a more powerful low-inertia brushed DC motor (Maxon RE 040). The motor applies torque to the joystick through a capstan drive with a gear ratio of 20:1.

An encoder coupled to the joystick reads angular joystick position for the computer controller with a resolution of 4096 counts per revolution. The angular workspace of the joystick is $\pm 30°$. In practice, however, angular displacements of the joystick did not exceed $\pm 10°$. An accelerometer was mounted to the joystick housing which in turn is fixed to the platform. In addition, the joystick handle was configured with a force sensor that measures the lateral force acting on the joystick or moment about the joystick axis. Also, a peg can be inserted through the handle and joystick housing to fix the joystick in its vertical position. Analog anti-aliasing filters were used on the platform acceleration $\ddot{x}_v$ and joystick force $f_b$ signals before sampling into the digital computer.

A 15 inch monitor was placed on a fixed desk 1.5 meters in front of the human subject for use as a tracking display. This distance was selected to remove the effects of relative motion on tracking performance [1]. The target and cursor were animated on the display in 1mm thick white lines on a black background. A 30 mm square box moving with the reference signal $x_r$ indicated the target and a similarly sized diagonal cross indicated the moving platform position $x_v$, as commanded by the joystick displacement. Both objects moved horizontally on the screen. The cursor representing platform position moved by 16cm on the screen for every 1cm of platform displacement.

**Control Design**

The platform and joystick were interfaced to a personal computer through a data acquisition and control card. During the experiments, the control program ran on the PC with a 1000 Hz servo rate under a real-time extended DOS kernel. All measured or actuated signals were sampled at $100$ Hz and recorded first to memory then to disk. Using digital control, the joystick and platform hardware were augmented with certain virtual elements that we now describe. In effect, these software additions gave the hardware the behavior modeled in the transfer functions of Figure 1.

Using the angular encoder and motor on the joystick, a virtual spring of stiffness $1.5$ Nm/rad with a vertical rest position was added by servo-control on the joystick. This gave the joystick a return-to-center behavior typical of many displacement sticks. The gain $C_p$ that determines the amount of platform displacement for a given joystick displacement was programmed with a fixed value of $0.11$ m/rad. A disturbance signal $d$ could be synthesized on the computer and added to the joystick command.

To model the dynamics of a vehicle, the inherent dynamics of the platform hardware and inner-loop position controller were augmented with a pure time delay. Several studies [19], [23], [24], [6] describe time delays in vehicle control systems in the range of $0.05 - 0.3$ seconds. To account for such delays, the studies [10] and [19] added software delays in experimental equipment. We added a 0.2 second delay to the position command signal. The platform and the delay together constitute our vehicle model $V$.

The position following performance of the platform was characterized in a preliminary system identification experiment. Filtered white noise was used for the position command input and the motor resolver reading was the output. Because the mass of the human subject is significant compared to that of the platform, a subject was seated in the platform during the tests. The experimental data yielded the transfer function estimate plot in Figure 4. The magnitude plot runs flat at $0$ dB up to about $10$ Hz, which covers our frequency range of interest. The phase plot reveals a lag that increases with frequency due to the delay term.

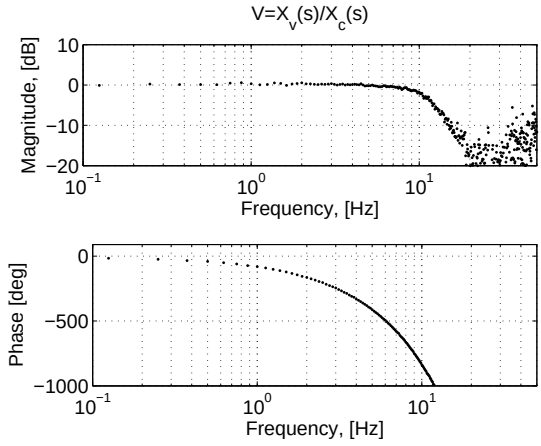


Fig. 4. Transfer function estimate of the platform $V$.

### A. System identification test

A significant feature of our approach to biodynamic feedthrough cancellation is the use of a system identification test that produces an estimate $\hat{H}$ of the biodynamic system $H$. The system identification experiment relies on an excitation

signal in the form of sufficiently rich vehicle motion and a measure of the biodynamic force $f_b$. In practice, the excitation signal is produced by vehicle ride motion.

Since the joystick force sensor measures the total force $f$ rather than the biodynamic force $f_b$ (see Figure 1), we applied two conditions that are designed to null the joystick driving point impedance response $f_{jb}$ and the volitional force $f_t$ during system identification. The first is to fix the joystick handle position to vertical by inserting a peg into the mechanism. Thus the joystick is reconfigured as a stiff-stick and the joystick angular velocity $\dot{x}_j$ and response force $f_{jb}$ are nulled. The second, to quell the force $f_t$, involves instructions to the human subject to simply hold the joystick handle without attempting to accomplish anything and elimination of the target and cursor from the screen. As long as these two conditions are set, the model $\hat{H}$ of the transfer function $H$ from vehicle acceleration $\ddot{x}_v$ to biodynamic force $f_b$ is equal to that from vehicle acceleration to total joystick force $f$. Our system identification experiment stipulates that the biodynamic system model equals the fraction on the right hand side of Equation 2, when evaluated under the two conditions specified.

$$\hat{H}(s) = \left. \frac{F(s)}{s^2 X_v(s)} \right|_{\dot{x}_j=0,\ f_t=0} \tag{2}$$

*1) Participants:* Twelve human subjects were recruited from the engineering graduate student body and each provided informed consent according to University of Michigan human subject protection policies.

*2) Experiment design:* The system identification experiment required only two minutes of participation from each subject. Each subject held the joystick in his or her hand without imposing force by volition and with the joystick fixed in vertical position by the peg.

To excite the biodynamic system $H$, the platform followed a filtered white noise position signal injected through $d$ that was bandpass filtered between 0.7 and 4 Hz. The maximum platform acceleration was 0.95 g's with a root-mean square average of $2.3\,\mathrm{m/s^2}$. The joystick force $f$ and the platform acceleration $\ddot{x}_v$ signals were sampled and recorded. Before further processing, the input and output signals were digitally low-pass filtered with a fifth order Butterworth filter tuned to $10\,\mathrm{Hz}$ and down-sampled to $50\,\mathrm{Hz}$ afterwards.

*3) Data Analysis:* Pilot study results indicated that biodynamic system estimates for our various human subject shared many features. These features allowed us to prescribe certain portions of linear time invariant (LTI) models to be fit to the data from each subject. In particular, we prescribed the order and relative order of the generic LTI model using observations of the number of peaks in the magnitude frequency response and shape of the phase frequency response of the biodynamic system estimate. Typically, the magnitude plot has two resonant peaks between $1\,\mathrm{Hz}$ and $8\,\mathrm{Hz}$, separated by a anti-resonance at about $5\,\mathrm{Hz}$. Accordingly, we chose a fourth order model. Higher order models did not yield more accurate fits. Because the magnitude plot is typically flat both at high frequencies, and the phase plot typically starts and returns to $180^\circ$, a relative degree of zero was chosen. Because the model is to be implemented in a discrete-time system, the system identification calculations were also carried out in discrete time, yielding an LTI difference equation with four poles and four zeros, according to the following model structure:

$$\underline{f}_b(n) = \sum_{i=0}^{4} \underline{\ddot{x}}_v(n-i) \cdot c_i - \sum_{j=1}^{4} \underline{f}_b(n-j) \cdot d_j \tag{3}$$

where parameters $c_i$, $(i = 0, 1, \ldots, 4)$ and $d_j$, $(j = 1, \ldots, 4)$ are constant, the acceleration $\ddot{x}_v$ and the force $f_b$ are discrete-time signals and $n$ indexes the samples. Our goal is to determine the constants $c_i$ and $d_j$ from the experimental data. To rewrite Equation 3 in matrix form, we define the data matrix $A$ and the parameter vector $\underline{b}$ as

$$A = [\underline{\ddot{x}}_v(n), \ldots, \underline{\ddot{x}}_v(n-4), -\underline{f}_b(n-1), \ldots, -\underline{f}_b(n-4)] \tag{4}$$

$$\underline{b} = [c_0,\ \ldots,\ c_4,\ d_1,\ \ldots,\ d_4]^T \tag{5}$$

where the underline indicates column vectors of discrete data and the arguments indicate shifting the data vector back in time. These definitions allow us to rewrite Equation 3 in the well-known matrix pseudoinverse form:

$$\underline{b} = (A^T\ A)^{-1}\ A^T\ \underline{f}_b \tag{6}$$

which yields a linear least-squares solution for the constants $c_i$ and $d_j$ in vector $\underline{b}$ and in Equation 3. Further details concerning data processing can be found in [7].

### *B. Tracking tests*

To assess the impact of the cancellation controller, we asked the same 12 subjects to perform a tracking task, using the joystick to move the platform and cursor on the screen. In half of the trials, a compensator produced a biodynamic cancellation force $\hat{f}_b$ that was applied to the joystick through the joystick motor. A compensator individually tailored to each subject was constructed according to the method described above in subsection III-A.

*1) Experiment design:* During the tracking tasks, the subjects controlled the platform with the joystick such that the platform position would follow a random-appearing tracking reference signal. A target and cursor representing the instantaneous values of the tracking reference signal and the platform position were displayed on a monitor (see Figure 3). A pursuit tracking task was constructed without preview. In one condition, tracking tasks were carried out without a compensator. In the other condition, tracking was performed with the compensator active. The conditions were presented in randomized order to average out learning and fatigue effects.

To obtain the best estimate for the human operator as a tracking controller, the tracking reference signal $x_r$ must be chosen carefully. Since the human tracking controller is assumed to be a quasi-linear system, superposition facilitates the computation of the describing function at a collection of frequencies if a sum of sinusoids of the same frequencies is used as a tracking reference signal. We chose a sum of 15 sinusoids with frequencies that were each prime multiples of

a fundamental frequency and with phase angles randomized at the beginning of each test. The randomization of phase angles eliminates precognitive tracking. The amplitudes and frequencies of the sinusoids were selected as given in [7].

In pilot studies, oscillations in the human/vehicle system arose often, exhibited as repeating back and forth movements of the joystick and platform. These oscillations would arise spontaneously when the subject produced fast tracking motions. The appearance of these oscillations would significantly deteriorate tracking performance, so the subjects attempted to avoid them. Usually, the subjects sacrificed tracking performance, choosing to follow only the low frequency components of the reference signal. The subjects managed to stabilize the system against changes in the tracking reference signal and suppress oscillations. However, the tracking reference signal is not the only external input to the human-machine system. In practice, environmental disturbance acting on the vehicle, e.g. gusts of wind, may initiate oscillatory or unstable response too. To reproduce such conditions in our experiment, we added an exogenous disturbance signal $d$ to the platform position command $x_c$. The disturbance signal was synthesized white noise band-pass filtered between $0.5$ and $4$ Hz with a root mean square average of $1.6\,\mathrm{m/s^2}$ and a peak value of $7.4\,\mathrm{m/s^2}$ and enveloped with a periodic waveform generated using a raised cosine wave. The result was a filtered white noise burst of four seconds that occurred every twenty seconds. The four second burst was sufficient to start oscillations, while the sixteen seconds between the bursts was used to observe the transient behavior: whether the oscillations were sustained, attenuated, or amplified over time.

*2) Participants:* Twelve test subjects, ten men and two women, aged 22-31 participated in the tracking experiment; the same twelve subjects who participated in the system identification experiment. Each subject‘s participation was confined to one day. Each subject had several hours of prior experience performing tracking tasks on the motion platform. Each subject was given at least three minutes of additional practice time before each task to further decrease learning effects.

*3) Performance Metrics:* We defined four performance metrics to quantify tracking performance and the presence of oscillatory behavior in the human/vehicle system.

**RMS error**

The average root mean square (RMS) tracking error is one of the most frequently encountered time domain performance metrics in the literature. We computed an average RMS error, but over only certain portions of the 180 second interval of each trial. Since we are primarily interested in the transient response that occurs during the 16 second intervals during which there was no disturbance, we first excised the 4 second windows from the data before computing the average RMS error. The RMS error was then also computed for the remaining 4 second intervals of the disturbance separately.

**Dwell ratio**

The dwell ratio $r_d$ is defined as the ratio of the accumulated time that the cursor center lies inside the target box to the total test time. This metric does not penalize errors below the target half-width, and parallels the performance metrics used in [25] and [26]. As with the RMS error, the dwell ratio was computed separately for the intervals while the disturbance was on and off.

**Crossover frequency**

The crossover frequency $f_c$ was defined in the frequency domain according to a fit of the crossover model (Eq. 1) to the forward path tracking signals $x_e$ and $x_v$. The crossover frequency indicates the bandwidth of the human tracking controller [27]. Following references [28], [29], [30], [4] and [31], we obtain the open-loop transfer function of the tracking loop as the cross-correlation spectral density of the signals $x_e$ and $x_v$ divided by the power spectral density of $x_e$. This computation is carried out for the fifteen frequencies used in the the sum of sinusoids reference signal, yielding 15 magnitude and phase values. A straight line with a $-20$ dB/decade slope was fit to the dots on the magnitude plot, then the $0$ dB intercept of the line was taken as the crossover frequency. The crossover frequency was computed for the entire $180s$ trial period. Further details concerning data processing can be found in [7].

**PSD integral**

We defined a fourth performance metric, naming it PSD integral, to quantify the presence of system oscillations based on the Power Spectral Density (PSD) magnitude plot of the joystick angle. Based on pilot study data, the PSD magnitude plot of the joystick angle signal features peaks between $1$ Hz and $7$ Hz if the human-machine system is oscillatory. We numerically integrated the PSD magnitude plot between integration limits from $1$ to $7$ Hz. The power spectral density of the joystick angle signal and PSD integral were computed for the entire $180s$ test time.

We interpret a low RMS error, a high dwell ratio and a high crossover frequency as indicators of good tracking performance, and a low PSD integral as an indicator of suppressed oscillations. The RMS error, the dwell ratio, the crossover frequency and the PSD integral values obtained for the twelve subjects with and without cancellation were compared using paired t-tests. A threshold value of $\alpha = 0.05$ was used to test for significance.

## IV. Results

The system identification experiment yielded a tailored cancellation controller for each subject. The second experiment was used to test the effectiveness of the cancellation controller in a simulated vehicle control task.

### A. System Identification Experiment

The transfer function estimate relating the biodynamic force $f_b$ to vehicle acceleration $\ddot{x}_v$ for a typical subject is shown as a swath of dots in Figure 5. This estimate was produced using the MATLAB `tfe` function on the experimental data. A model in the form of Eq. (3) was fit in the time domain using the method of least squares (Eq. (6)). The resulting model is presented overlayed as a continuous line in Figure 5.
Individual model fits were performed for each of the twelve subjects. Figure 6 shows the models in the frequency domain for all twelve subjects overlayed.

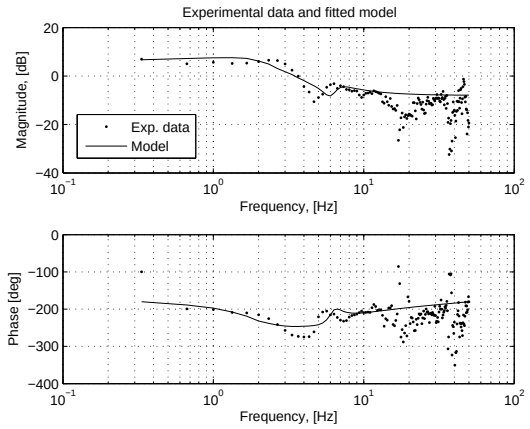


Fig. 5. The experimental transfer function estimate for the biodynamic system $H$ of a representative subject is shown in dots while a frequency-domain representation of the model $\hat{H}$ that was fit to the data is shown in the continuous line.

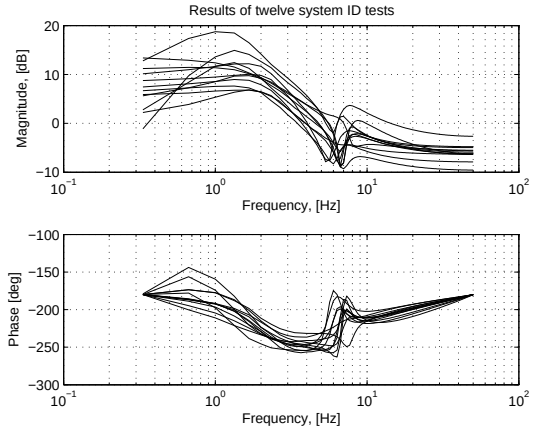


Fig. 6. Comparison of biodynamic system models obtained for all the twelve subjects.

The model fits vary significantly across subjects. Note that some of the common features are determined by the structure of the model. In particular, because the models have a relative order of zero, the magnitude plots are flat at high frequencies and the phase plots start and end at $-180°$. This agrees with our sign convention for the direction of the joystick force and platform displacement and with the notion that the inertia force opposes acceleration.

### *B. Tracking Experiment*

Data from the tracking experiment indicate that the biodynamic feedthrough compensator significantly enhanced tracking performance. A brief 20-second window of the reference signal $x_r$ and the platform displacement $x_v$ are shown in the upper graph in Figure 7. The lower graph indicates the disturbance $d$ that was added to the joystick command signal to incite oscillations and test the system disturbance response. The hatched area in both graphs indicates the 4-second window in which the disturbance was non-zero. Note that the response $x_v$ exhibits an oscillatory behavior, with a fundamental frequency around $2.5$ Hz. The oscillations are not only sustained after the disturbance vanishes, but also reappear after a brief three second intermission during seconds 112 through 116.

A similar pair of graphs is shown in Figure 8 for the same subject when the compensator was turned on. The amplitudes of the oscillations are smaller during the 4 second period when the disturbance excites the system. The oscillations disappear and tracking is restored after the disturbance returns to zero.

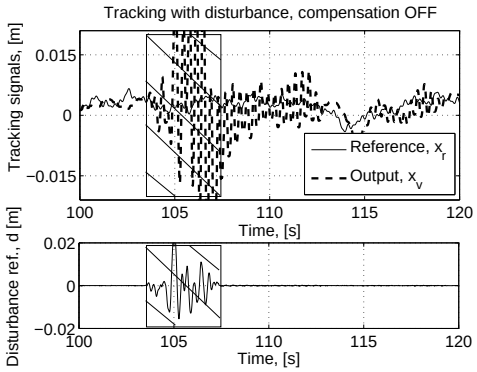


Fig. 7. Time domain signals of an uncompensated tracking task

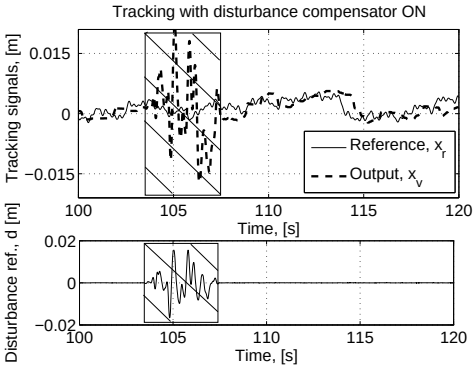


Fig. 8. Time domain signals of a compensated tracking task

To quantify the tracking error, we first collapsed the seven 20-second periods within each 180 second trial that each included 4 seconds of disturbed tracking followed by 16 seconds of undisturbed tracking. The first disturbance period was excluded due to startup, the last one was incomplete, which left us with seven to include. We then computed the RMS error across the 7 periods and across the 12 subjects to produce a single 20-second RMS error trace for each of the two conditions, with and without compensation. The RMS error traces for each condition are shown versus a generalized time from 0 to 20 seconds as two graphs in Figure 9. The gray area behind the solid line indicating the mean extends one standard deviation above and below the mean.

Whether the compensator is present or not (panes A and B of Figure 9), the tracking error is high during the first four seconds while the disturbance is turned on (shown in the hatched region). The error decreases during the remaining sixteen seconds of undisturbed tracking. Comparing panes A and B, one recognizes that the compensator reduces both the mean and the standard deviation of the RMS error, across the

12 subjects. Pane C presents a boxplot of the RMS average tracking error computed for the undisturbed time periods only. In all of the box-and-whisker plots in this paper the box encloses the upper and lower quartiles, a middle line corresponds to the median, and the whiskers indicate the range of the data.

To facilitate computation of the dwell ratio $d_r$ and a presentation of a 20-second trace analogous to the RMS error traces in Figure 9, an indicator function was defined to return a $1$ when the cursor center was inside the target box and a $0$ otherwise. The mean and standard deviation of the indicator function was computed for the twelve subjects and the seven disturbance periods. Each average displays the four seconds of disturbed tracking between 0s and 4s followed by the remaining $16s$ of undisturbed tracking.

Figure 10 shows the dwell ratio for the uncompensated condition in Pane A and the compensated condition in Pane B. The graph on pane B is noticeably lower, especially during the 16 second undisturbed period, indicating longer time spend on-target. The boxplot testifies to a diminished scatter and an increase in the mean of the dwell ratio values, indicating that the compensator improved tracking performance.

Panes A and B in Figure 11 present the PSD magnitude plot of the joystick angle $x_j$ for a sample subject without and with cancellation, respectively. The plot corresponding to uncompensated tracking features two distinct peaks at $2.5$ Hz and at $5.5$ Hz, which correspond to two oscillation modes. These peaks disappear when the cancellation controller is turned on. The PSD magnitude plot drops by over $50$ dB at $2.5$ Hz, and by about $35$ dB at $5.5$ Hz as a result of compensation, indicating suppression of oscillations. Pane C shows the boxplot of the PSD integrals computed for the twelve subjects. The PSD magnitude drops as a result of cancellation.

Panes A and B in Figure 12 illustrate the open-loop transfer function of the tracking loop, $\frac{X_v(j\omega)}{X_e(j\omega)}$, computed for the frequencies of the fifteen sinusoids of the tracking reference signal for a sample human subject. Pane A illustrates tracking without compensation, while pane B corresponds to compensated tracking. A straight line of slope $-20$ dB/decade was fit on the dots of the magnitude plot in the frequency domain. The $0$ dB intercept of the line yielded the crossover frequencies shown at the top of the plots. As shown by the plots in panes A and B, the crossover frequency increased for this subject as a result of using the compensator. A boxplot of the crossover frequencies obtained for the twelve subjects for the uncompensated and the compensated tests is shown in pane C. As the plots manifest, the compensator increases the crossover frequency.

Table I lists the average performance metrics computed across the twelve subjects for compensated and uncompensated tracking. The computations for the RMS error and dwell ratio $r_d$ were performed separately for the disturbed (denoted $d$) and the undisturbed (denoted $nd$) sections of the test. Also indicated are the p-values obtained from the paired t-tests used to compare the performance metric values obtained with and without compensation. The RMS error values computed both for the disturbed and the undisturbed sections decrease as a result of compensation. The dwell ratio increases in both cases, along with the crossover frequency. The average of the PSD integral across the twelve subjects also decreases due to the use of the cancellation controller. All comparisons resulted in p-values less than 0.05, or achieved statistical significance.

TABLE I

COMPARISON OF PERFORMANCE METRICS COMPUTED FOR UNCOMPENSATED AND COMPENSATED TRACKING TASKS.

| Perf. metrics | No comp. | Comp. | p-value |
|---|---|---|---|
| $RMS$ error, [mm] (d) | 97 | 82 | $<$0.001 |
| $RMS$ error, [mm] (nd) | 37 | 20 | 0.0053 |
| $r_d$ (d) | 0.105 | 0.120 | 0.011 |
| $r_d$ (nd) | 0.34 | 0.39 | 0.021 |
| $f_c, [Hz]$ | 0.15 | 0.17 | 0.095 |
| $PSD$ int. | -892 | -971 | $<$0.001 |

This concludes the presentation of our experimental results. Let us now continue with discussion.

## V. DISCUSSION

### A. System identification test

The identified biodynamic system models have several features in common, but they also vary across different subjects. The variation is a result of the interplay of several factors, including the body type and posture of the test subject, the restraints used, the length of the joystick, the direction of joystick axis, and the time variation of stiffness of various muscles in the subjects body. The strength of grip and various stretch reflexes also influence the biodynamic model. This leads us to believe that the model depends both on the subject and on the vehicle.

Due to the differences between the models obtained for our twelve subjects, we currently use a separate controller for each subject. Further research may facilitate the creation of a single controller for all subjects.

### B. Tracking tests

The effectiveness of the cancellation controller was verified in human subject tests. A joint experiment of tracking and disturbance rejection was carried out with and without the cancellation controller on twelve human subjects. A sum of sinusoids tracking reference signal and a motion disturbance made up from periodic, occasional bursts of filtered white noise excited the human-machine system simultaneously.

To best investigate the oscillatory nature of the system, attention was paid to replicate the dynamics of real vehicles with the platform. The electrohydraulic servo system of aircraft control flaps introduces a delay into vehicle response, this is reported to be somewhere between 0.05sec and 0.3sec [23], [24], [6]. The experimental apparatus of some past investigations on vibration feedthrough [10] use a 0.08sec artificial delay to account for this. We used a 0.2sec delay. Biodynamic feedthrough would deteriorate manual control performance even if the delay was not present, but the system would be less oscillatory.

Our goals were twofold, we aimed to suppress the oscillations and improve tracking performance. The changes

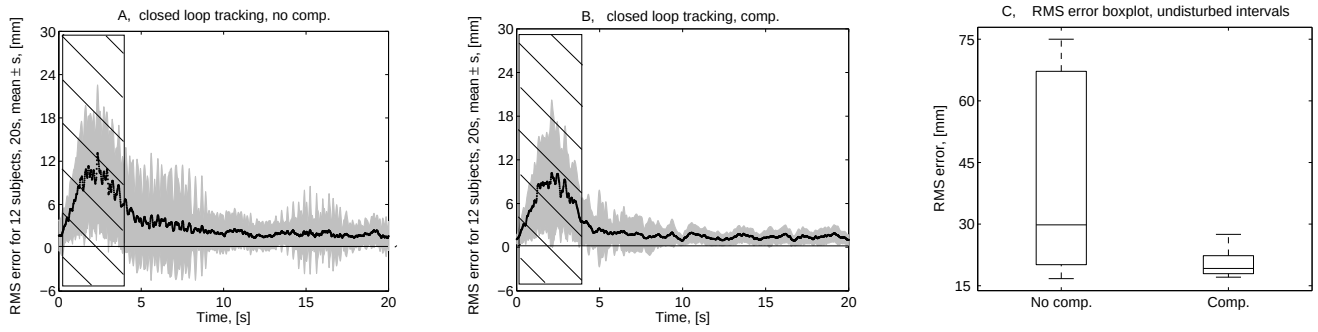


Fig. 9. RMS error averages under the two test conditions

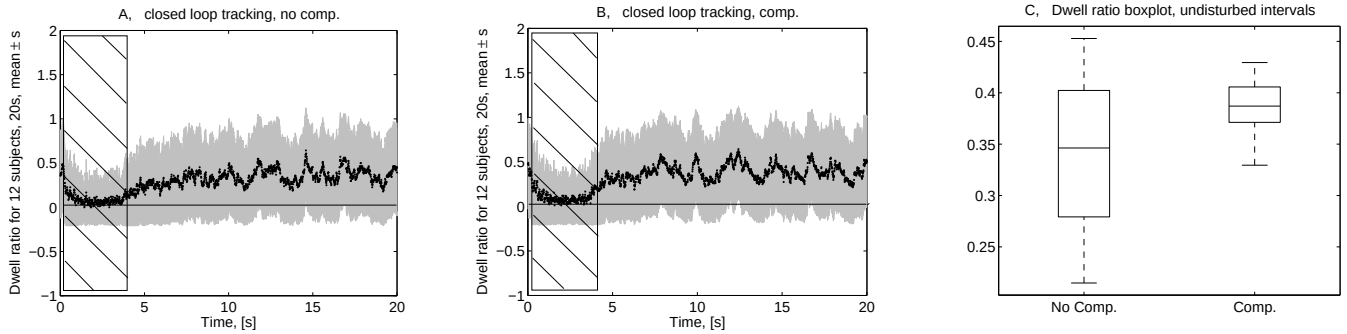


Fig. 10. Dwell ratio time averages under the two test conditions

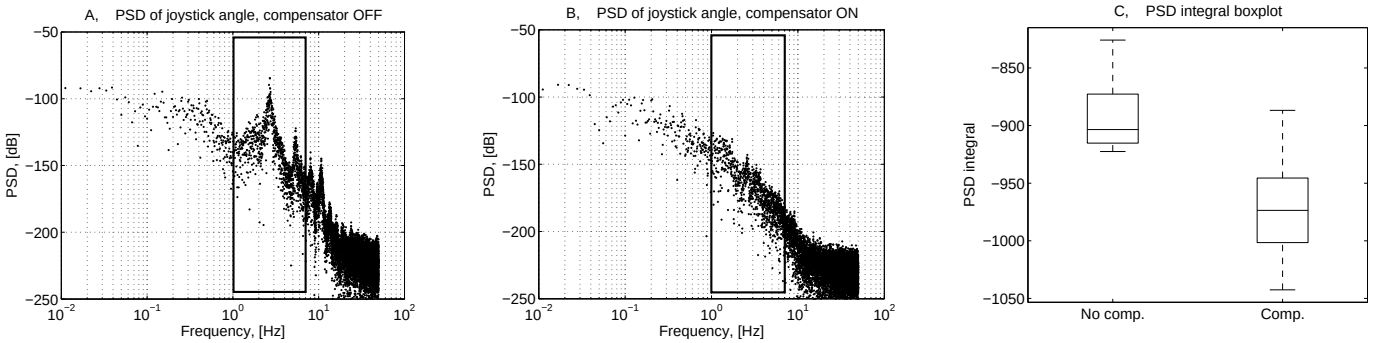


Fig. 11. PSD plots of joystick angle for one particular subject and PSD boxplot for the 12 subjects.

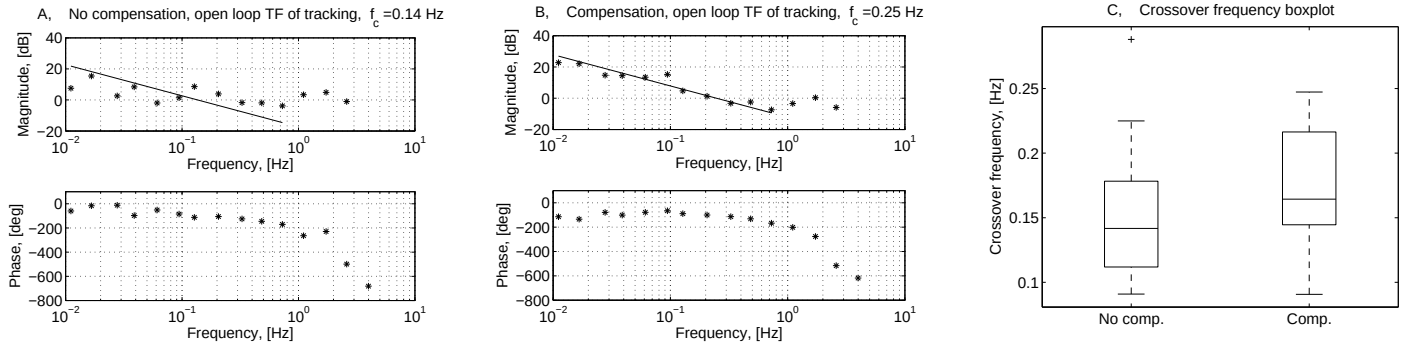


Fig. 12. Crossover models for one particular subject and crossover frequency boxplot for the 12 subjects.

in performance metrics show the beneficial effects of the controller on the system.

Both the mean and the standard deviation of the RMS error computed for the twelve subjects drops as a result of using the controller, these signify improved tracking. The increase of the RMS error is significant when computed both for the time intervals with and without disturbance. This evidences tracking performance improvement as a result of cancellation.

The dwell ratio shows similar trends. The mean of the dwell ratio computed both for the disturbed and undisturbed sections of the tests increases as a result of using the cancellation controller. As the p-values show, these changes are statistically significant, which allows us to conclude that the cancellation controller improves tracking performance.

The crossover frequencies computed for the twelve subjects under the two test conditions also show tracking performance improvement, although the p-value is greater than our significance level of $\alpha = 0.05$. The increase in crossover frequency indicates an increase in the bandwidth of the closed-loop human-machine system, which evidences performance improvement.

A curious feature of the crossover models corresponding to tracking carried out in a moving platform is the raise of the magnitude plot around 1.5-2Hz. In a study [19], where the biodynamic system model has a peak in this frequency range, the peak of the biodynamic system model is a basis for explaining the peak in the open-loop transfer function of tracking at the same frequency. Our biodynamic models built based on human subject test data also have a peak around 2Hz, which may explain the peaks we also see on the magnitude plots on panes A and B in Figure 12.

The use of the cancellation controller removes several oscillatory peaks from the PSD magnitude plots of the joystick angle signal. In some cases, as for example in Figure 11, this implies an over $40dB$ drop in magnitude, corresponding to a drop to less than one percent of the value of the uncompensated case. Besides examples of individual test results, summary results were also used to demonstrate the effect of the controller. The performance metric introduced to quantify joystick angle signal energy in the 1-7Hz frequency band, the PSD integral also drops as a result of using the cancellation controller. As the p-values indicate, the drop is significant at a significance level of $\alpha = 0.05$. The human subjects also noted that the oscillatory response of the human-machine system was greatly suppressed by the solution proposed.

## VI. Discussion and Conclusions

According to multiple performance metrics, cancellation controllers individually fit to the transmittance from vehicle acceleration to joystick force significantly improved pursuit tracking performance and improved disturbance response. Cancellation reduced the RMS tracking errors in the undisturbed test intervals by 44 %. The mean dwell ratios computed for the undisturbed test intervals increased by 16 %, indicating that cancellation increased time spent on-target. The crossover frequencies computed for the twelve subjects reflect increased driver-vehicle system bandwidth, or tracking performance improvement with the cancellation controller in place, although the p-value was greater than our significance level of $\alpha = 0.05$. Finally, the cancellation controller produces a reduction by 12 dB in power spectral density of joystick motion in the 1-7 Hz range compared to the uncompensated values. The subjects also reported in post-experiment interviews that oscillations were suppressed in certain trails and that their tracking performance was noticeably improved. The subjects indicated that they noticed that the joystick felt different in certain experiment trials, but that this action was not distracting nor uncomfortable.

Note that there is a peak in the crossover magnitude plot around 1.5-2Hz (see Figure 12). As noted in reference [19], this peak is related to the peak in the same frequency band in PSD joystick angle (see Figure 11). It is also present in the biodynamic system model (Figure 6. Also noteworthy is a trend that is not reflected in the summary results reported above: that the cancellation controller produced benefit for all 12 subjects and all four performance metrics. That is, the differences in performance produced by the cancellation controller had the same sign (reflecting improved performance) for all subjects.

The identified biodynamic system models have several features in common across subjects, such as the consistent appearance of a notch between two peaks in the frequency response plot (see Figure 6. But the frequency at which that notch appears varied between 5 and 7 Hz across subjects. Factors that may contribute to such variation include differences in anthropometry between subjects or variations in posture adopted during the experiment. The restraints might function differently for each subject, or their function might even be influenced by clothing. Also, differences in grip and nominal muscle activation adopted by each subject during the system identification experiment may affect the resonant frequency or magnitude of a vibration mode within some portion of the kinematic chain comprising torso, upper and lower arm, and hand. The present experiment did not use a physically-based multibody model nor was motion tracking of the body segments available, so we do not know the association between certain features in the frequency response and vibration modes in the body.

Whatever their etiology, the appearance of variation in the features of the biodynamic models fit to our twelve subjects prompted us to use an individualized cancellation controller for each subject. We have anecdotal evidence showing that a controller designed for one subject does not necessarily function well for another subject. However, further investigation is needed to determine what benefits might be lost if a single, population average controller were to be used for all subjects, or whether a single controller could be successfully parameterized, say, by stature and/or weight. The use of an average controller would remove the need for the force sensor on the joystick and the preliminary system identification experiment. Of course another approach that would eliminate the system identification step is the formulation of an adaptive controller. On-line system identification could be used to adapt a nominal initial controller to the biodynamic response of particular subjects. A time-varying controller that continually adapted to the transmittance would account for time-varying features such as those due to changes in grip or posture adopted during control by a single subject. Alternatively, the controller could be parameterized by grip force and could be tuned on-line according to grip force measurements. These extensions, however, remain future work in our lab.

## VII. Acknowledgments

The authors would like to express their gratitude to the test subjects who spent many hours on the platform. Also many thanks to our sponsor, the Automotive Research Center at the University of Michigan. Thanks are also due to Wright Patterson Air Force Base for loaning us the single-axis motion platform.

## REFERENCES


[1] R. W. McLeod and M. J. Griffin, "Mechanism of vibration-induced interference with manual control performance," *Ergonomics*, vol. 38, no. 7, pp. 1431–1444, 1994.

[2] F. Arai, J. Tateishi, and T. Fukuda, "Dynamical analysis and suppression of human hunting in the excavator design," *Proceedings of the 2000 IEEE International Workshop on Robot and Human Interactive Communication, Osaka, Japan*, September 27-29 2000.

[3] N. R. Parker, S. E. Salcudean, and P. D. Lawrence, "Application of force feedback to heavy duty hydraulic machines," pp. 375–381, 1993.

[4] R. Hess, "Theory of roll-ratchet phenomenon in high performance aircraft," *Journal of Guidance, Control and Dynamics*, vol. 21, no. 1, pp. 101–108, Jan-Feb. 1998.

[5] D. Banerjee, L. M. Jordan, and M. J. Rosen, "Modeling the effects of inertial reactions on occupants of moving power wheelchairs," *Conference of the RESNA, Proceedings of the Rehabilitation Engineering and Assistive Technology Society of North America*, p. 88, 1996.

[6] D. T. McRuer, *Pilot-Induced Oscillations and Human Dynamic Behavior*. NASA Contractor Report 4683: National Aeronautics and Space Administration, July 1995.

[7] R. Gillespie and S. Sövényi, "Model-based cancellation of biodynamic feedthrough using a force-reflecting joystick," *ASME Journal of Dynamic Systems, Measurement and Control*, p. Submitted for publication, 2005.

[8] R. B. Gillespie, C. Hasser, and P. Tang, "Cancellation of feedthrough dynamics using a force-reflecting joystick," *Proc. ASME Dynamic Systems and Controls Division*, pp. 319–326, 1999.

[9] S. Sövényi and R. Gillespie, "An investigation of vibration feedthrough and feedthrough cancellation in joystick controlled vehicles.," *2003 International Mechanical Engineering Congress and R and D Expo, IMECE2003-41598, Washington, D.C. USA, ASME Dynamic Systems and Control Division, DSC*, vol. 72, no. 1, pp. 567–576, 2003.

[10] M. Sirouspour and S. Salcudean, "Suppressing operator-induced oscillations in manual control systems with movable bases," *IEEE Transactions on Control Systems Technology*, vol. 11, no. 4, pp. 448–459, July 2003.

[11] H. R. Jex and R. E. Magdaleno, "Biomechanical models for vibration feedthrough to hands and head for a semisupine pilot," *Aviation, Space and Environmental Medicine*, pp. 304–316, January, 1978.

[12] M. Verger, A. Grunwald, and S. Merhav, "Suppression of biodynamic disturbances and pilot-induced oscillations by adaptive filtering," *Journal of Guidance*, vol. 7, no. 4, pp. 401–409, July-August 1984.

[13] M. Verger, A. Grunwald, and S. Merhav, "Adaptive filtering of biodynamic stick feedthrough in manipulation tasks on board moving platforms," *Journal of Guidance*, vol. 11, no. 2, pp. 153–158, march-April 1988.

[14] M. R. Sirouspour and S. E. Salcudean, "Robust controller design for canceling biodynamic feedthrough," *8th International Symposium on Experimental Robotics, ISER*, July 8-11, 2002.

[15] G. J. Jeram and J. V. R. Prasad, "Tactile avoidance cueing for pilot induced oscillation," *AIAA Atmospheric Flight Mechanics Conference, AIAA-2003-5311*, pp. 129–137, Aug. 11-14, 2003.

[16] R. A. Hess and B. D. McNally, "Automation effects in a multiloop manual control system," *IEEE Transactions on Systems, Man and Cybernetics*, vol. SMC-16, no. 1, pp. 111–121, 1986.

[17] D. W. Repperger, "Smart stick controllers," *Proceedings of the American Control Conference*, vol. 2, pp. 807–812, 1983.

[18] D. W. Repperger and L. Rothrock, "Using ga-based intelligent control means to enhance human-machine interfaces," *Intelligent Automation and Soft Computing*, vol. 10, pp. 1–18, 2004.

[19] D. E. Johnston and D. T. McRuer, "Investigation of limb-side stick dynamic interaction with roll control," *Journal of Guidance*, vol. 10, no. 2, pp. 178–186, March-April 1987.

[20] T. B. Sheridan and W. R. Ferrell, *Man-Machine Systems: Information, Control and Decision Models of Human Performance*. The MIT Press, first edition ed., 1974.

[21] D. T. McRuer and H. R. Jex, "A review of quasi-linear pilot models," *IEEE Transactions on Human Factors in Electronics*, vol. HFE 8, no. 3, pp. 231–249, September 1967.

[22] R. W. Allen and H. R. Jex, "A simple fourier analysis technique for measuring the dynamic response of manual control systems," *IEEE Transactions on Systems, Man, and Cybernetics*, vol. SMC-2, no. 5, pp. 638–643, 1972.

[23] E. N. Bachelder and D. H. Klyde, "Wavelet-based analysis of roll ratchet using a flight test database," *Atmospheric Flight Mechanics Conference, Austin, Texas*, no. Paper No. 607, pp. 1–11, 11-14 August 2003.

[24] D. G. Mitchell, B. L. Aponso, and D. H. Klyde, *Effects of Cockpit Lateral Stick Characteristics on Handling Qualities and Pilot Dynamics*. NASA Contractor Report 4443: National Aeronautics and Space Administration, June 1992.

[25] D. W. Repperger, C. A. Phillips, J. E. Berlin, A. T. Neidhard-Doll, and M. W. Haas, "Human-machine haptic interface design using stochastic resonance methods," *IEEE Transactions on Systems, Man and Cybernetics-Part A: Systems and Humans*, 2005.

[26] D. W. Repperger, S. L. Ward, E. J. Hartzell, B. C. Glass, and W. C. Summers, "An algorithm to ascertain critical regions of human tracking ability," *IEEE Transactions on Systems, Man and Cybernetics*, vol. SMC-9, no. 4, pp. 183–196, April 1979.

[27] D. McRuer, D. Graham, E. Krendel, and W. Reisener, "Human pilot dynamics in compensatory systems-theory, models and experiments with controlled element and forcing function variations," *AFFDL-TR-65-15*, July 1965.

[28] D. T. McRuer, R. W. Allen, D. H. Weir, and R. H. Klein, "New results in driver steering control models," *Human Factors*, vol. 19, no. 4, pp. 381–397, 1977.

[29] D. McRuer, "Human dynamics in man-machine systems," *Automatica*, vol. 16, pp. 237–253, 1980.

[30] R. A. Hess, "Analyzing manipulator and feel system effects in aircraft flight control," *IEEE Transactions on Systems, Man and Cybernetics*, vol. 20, no. 4, pp. 923–931, July/August 1990.

[31] D. Johnston and B. Aponso, "Design considerations of manipulator and feel system characteristics in roll ratcheting," *NASA CR-4111*, Feb. 1988.